ULTIMATE LOAD ANALYSIS USING FINITE ELEMENT METHODS

by

ARTHUR P. CIMENTO

SUBMITTED IN PARTIAL FULFILLMENT
OF THE REQUIREMENTS FOR THE
DEGREE OF

BACHELOR OF SCIENCE

at the

MASSACHUSETTS INSTITUTE OF TECHNOLOGY

April 1978

Signature redacted

Signature of Author.....
Department of Mechanical Engineering
April 1978

Signature redacted

Certified by.....
Thesis Supervisor

Signature redacted

Accepted by.....
Chairman, Departmental Committee on
Thesis

ULTIMATE LOAD ANALYSIS USING FINITE ELEMENT METHODS

by

ARTHUR P. CIMENTO

Submitted to the Department of Mechanical Engineering on April 28, 1978 in partial fulfillment of the requirements for the Degree of Bachelor of Science.

ABSTRACT

The analysis of ultimate load problems with the finite element method may involve difficulties due to the large geometric and material non-linearities that need be taken into account. A formulation for the analysis of problems involving large strain plasticity is presented and consideration is given to the difficulties encountered when incompressibility constraints are imposed in plasticity analysis. The determination of the limit load for a rigid punch indenting a half-space of perfectly-plastic material is examined as an illustration of both the difficulties involved in ultimate load analysis and the effect of different finite element models on the solution.

Thesis Supervisor: Klaus J. Bathe
Title: Associate Professor of Mechanical Engineering

ACKNOWLEDGMENTS

I would like to express my gratitude to Professor Klaus-Jürgen Bathe for his assistance and guidance during the research and preparation for this thesis. His suggestions were invaluable for the completion of this project.

I would like to thank Seshardi Ramaswamy, Walter Hahn and Said Bolourchi for their help during the research work. I would also like to express my appreciation for the efforts of Alfred Chock in drawing the figures for this thesis & Karen Rawlinson for the typing.

The continuous development and maintenance of ADINA is being supported by the ADINA users' group. I would like to acknowledge gratefully the support that the users' group has provided for our research and development efforts.

TABLE OF CONTENTS

LIST OF FIGURES

1. INTRODUCTION

The successful application of the finite element method to the solution of ultimate load problems has been demonstrated through a variety of analyses. Nayak and Zienkiewicz [1] performed elastic-plastic stress analyses to determine limit loads for several metal forming processes and the collapse load for a pressure vessel. Close agreement with experimental and theoretical results were obtained for both force and displacement boundary conditions. Application of this method to geomechanics problems, particularly in investigating the bearing capacity of foundations, has been investigated recently by Yamada and Wifi [2] and by Christian et al. [3], using very coarse meshes. Finite element formulations designed specifically for analyzing ultimate load problems have been developed and successfully implemented by a number of researchers [4-6]. In these formulations linear or non-linear programming techniques are used and they therefore differ from conventional elastic-plastic analysis techniques in their solution procedures. Rather than incrementally solve for the displacement field, these methods determine upper and lower bounds on the limit load through direct application of limit theorems (e.g. see Martin [7]) and attempt to minimize their difference. The application of these methods has been demonstrated on a number of problems [8].

An important consideration in the use of finite element techniques on this class of problems is the type of formulation to be used. The choice will depend on the particular problem and on the desired detail and accuracy required of the solution. This paper will investigate various aspects of

the elastic-plastic stress analysis techniques. The presence of both plastic regions undergoing large plastic straining and elastic regions in the same structure is a feature of ultimate load problems which requires special attention. Formulations which account for large strain plasticity may be necessary to describe the behavior of the plastic regions. The optimum integration order to use in isoparametric element analysis is also unclear. The effect of integration order on stress calculations becomes particularly important when such elements become fully plastic. Finally, the necessary detail in the finite element model to obtain accurate estimates of both the limit load and the stress and strain distributions through the structure needs to be examined.

The investigation outlined in this paper was performed on the two-dimensional plane strain element implemented in the ADINA program [9]. The example chosen was one whose classical solution is well known, a rigid flat punch indenting an infinite half space of elastic-perfectly plastic material. The punch problem is similar to many metal working applications (e.g. stamping operations) and geomechanics problems (e.g. bearing capacity of foundations).

2. LARGE STRAIN PLASTICITY FORMULATION

The large plastic strains which may be encountered in local areas of a structure as it approaches its limit load requires accounting for both geometric and material non-linearities. Finite element analyses using total or updated Lagrangian formulations for problems of large elastic-plastic deformations, such as those surveyed by Key, Biffle and Krieg [15], have been used with some success to model finite straining. Large strain elastic-plastic analysis in ADINA uses an updated Lagrangian formulation, which refers all static and kinematic variables to the configuration at the current time t. A complete derivation of the updated Lagrangian formulation used in ADINA can be found in [16], a summary of the derivation for static analysis can be found in Table 1.

2.1 Updated Lagrangian Formulation - Kinematics

For the updated Lagrangian formulation, the virtual work theorem can be written in incremental form (using Cauchy stress tensor τ_{ij})

$$\int_V \dot{\tau}_{ij} \dot{e}_{ij} \, dV = \dot{R} \tag{1a}$$

or, in the form

$$\int_{{}^tV} {}^{t+\Delta t}_{t}S_{ij} \, \delta \, {}^{t+\Delta t}_{t}\varepsilon_{ij} \, {}^{t}dV = {}^{t+\Delta t}R \tag{1b}$$

where ${}^tV$ is the volume of the body at time t, ${}^{t+\Delta t}_{t}S_{ij}$ is the 2nd Piola-Kirchhoff stress tensor at time t+Δt referred to the configuration at time t, ${}^{t+\Delta t}_{t}\varepsilon_{ij}$ is the strain increment tensor at time t, and ${}^{t+\Delta t}R$ is the external

TABLE 1. UPDATED LAGRANGIAN FORMULATION

1. Equations of Motion

$$\int_{t_V} {}^{t+\Delta t}_{t}S_{ij}\, \delta\, {}^{t+\Delta t}_{t}\varepsilon_{ij}\, {}^{t}dV = {}^{t+\Delta t}\mathcal{R}$$

where

$$ {}^{t+\Delta t}_{t}S_{ij} = \frac{{}^{t}\rho}{{}^{t+\Delta t}\rho}\left(\frac{\partial {}^{t}x_i}{\partial {}^{t+\Delta t}x_s}\right) {}^{t+\Delta t}\tau_{sr} \left(\frac{\partial {}^{t}x_i}{\partial {}^{t+\Delta t}x_r}\right) \quad (\rho \equiv \text{specific mass})$$

$$\delta\, {}^{t+\Delta t}_{t}\varepsilon_{ij} = \delta\left[\frac{1}{2}\left({}^{t}u_{i,j} + {}^{t}u_{j,i} + {}^{t}u_{k,i}\, {}^{t}u_{k,j}\right)\right]$$

2. Incremental Decompositions

a. stresses

$$ {}^{t+\Delta t}_{t}S_{ij} = {}^{t}\tau_{ij} + {}^{t}_{t}S_{ij}$$

b. strains

$$ {}^{t+\Delta t}_{t}\varepsilon_{ij} = {}^{t}\varepsilon_{ij}$$

$${}^{t}\varepsilon_{ij} = {}^{t}e_{ij} + {}^{t}\eta_{ij}$$

$${}^{t}e_{ij} = \frac{1}{2}\left({}^{t}u_{i,j} + {}^{t}u_{j,i}\right)$$

$${}^{t}\eta_{ij} = \frac{1}{2}\, {}^{t}u_{k,i}\, u_{k,j}$$

3. Equations of Motion with Incremental Decomposition

Using ${}^{t}_{t}S_{ij} = {}^{t}C_{ijrs}\, {}^{t}\varepsilon_{rs}$ the equations of motion become

$$\int_{t_V} {}^{t}C_{ijrs}\, {}^{t}\varepsilon_{rs}\, \delta\, {}_{t}\varepsilon_{ij}\, {}^{t}dV + \int_{t_V} {}^{t}\tau_{ij}\, \delta\, {}_{t}\eta_{ij}\, {}^{t}dV = {}^{t+\Delta t}\mathcal{R} - \int_{t_V} {}^{t}\tau_{ij}\, \delta\, {}_{t}e_{ij}\, {}^{t}dV$$

TABLE 1. (continued)

4. Linearized Equations of Motion

Using the approximations ${}_tS_{ij} = {}_tC_{ijrs}\ {}_te_{rs}$, $\delta\ {}_t\mathcal{E}_{ij} = \delta_t\ e_{ij}$, the approximate equations of motion are

$$\int_{{}_tV} {}_tC_{ijrs}\ {}_te_{rs}\,\delta_t\ e_{ij}\ {}^t dV + \int_{{}_tV} {}_t\tau_{ij}\,\delta\,{}_t\eta_{ij}\ {}^t dV = {}^{t+\Delta t}\mathcal{R} - \int_{{}_tV} {}_t\tau_{ij}\ {}_te_{ij}\ {}^t dV$$

virtual work at time t+Δt. The stresses can be decomposed into components of a Cauchy stress tensor at time t, ${}^{t}\tau_{ij}$, and the 2nd Piola-Kirchhoff stress tensor at time t, ${}_{t}S_{ij}$, as

$$ {}^{t+\Delta t}_{t}S_{ij} = {}^{t}\tau_{ij} + {}_{t}S_{ij} \tag{2} $$

while the strain increment tensor can be separated into a linear strain increment ${}_{t}e_{ij}$ and a non-linear increment ${}_{t}\eta_{ij}$ (both referred to the configuration at time t) as

$$ {}^{t+\Delta t}_{t}\varepsilon_{ij} \equiv {}_{t}\varepsilon_{ij} $$

$$ {}_{t}\varepsilon_{ij} = {}_{t}e_{ij} + {}_{t}\eta_{ij} \tag{3} $$

Introducing the incremental material property tensor referred to the configuration at time t, ${}_{t}C_{ijrs}$, and using the approximation ${}_{t}S_{ij} = {}_{t}C_{ijrs}\,{}_{t}e_{rs}$ and $\delta_t \varepsilon_{ij} = \delta_t e_{ij}$, the virtual work theorem can be rewritten, using Eqs. (2) and (3), as:

$$ \int_{{}^{t}V} {}_{t}C_{ijrs}\,{}_{t}e_{rs}\,\delta_t e_{ij}\,{}^{t}dV + \int_{{}^{t}V} {}^{t}\tau_{ij}\,\delta_t \eta_{ij}\,{}^{t}dV = {}^{t+\Delta t}\mathcal{R} - \int_{{}^{t}V} {}^{t}\tau_{ij}\,\delta_t e_{ij}\,{}^{t}dV \tag{4} $$

which is the linearized equilibrium equation used in the updated Lagrangian formulation. The finite element implementation of Eq. (4) can be written in matrix form as

$$\left({}^{t}_{t}\underline{K}_{L} + {}^{t}_{t}\underline{K}_{NL}\right)\underline{u} = {}^{t+\Delta t}\underline{R} - {}^{t}_{t}\underline{F} \tag{5}$$

where ${}^{t}_{t}\underline{K}_{L}$ and ${}^{t}_{t}\underline{K}_{NL}$ are the linear and nonlinear strain incremental stiffness matrices, $\underline{u}$ is the vector of incremental nodal displacements, ${}^{t+\Delta t}\underline{R}$ is the external nodal force vector, and ${}^{t}_{t}\underline{F}$ is the vector of nodal forces equivalent to the element stresses at time t. In terms of the integral formulation of Eq. (4), the terms of the matrix Eq. (5), approximate

$${}^{t}_{t}\underline{K}_{L}\,\underline{u} = \left(\int_{{}^{t}V} {}^{t}_{t}\underline{B}_{L}^{T}\,{}^{t}\underline{C}\,{}^{t}_{t}\underline{B}_{L}\,{}^{t}dV\right)\underline{u} \doteq \int_{{}^{t}V} {}^{t}C_{ijrs}\,{}_{t}e_{rs}\,\delta_{t}e_{ij}\,{}^{t}dV \tag{6}$$

$${}^{t}_{t}\underline{K}_{NL}\,\underline{u} = \left(\int_{{}^{t}V} {}^{t}_{t}\underline{B}_{NL}^{T}\,{}^{t}\underline{\tau}\,{}^{t}_{t}\underline{B}_{NL}\,{}^{t}dV\right)\underline{u} \doteq \int_{{}^{t}V} {}^{t}\tau_{ij}\,\delta_{t}\eta_{ij}\,{}^{t}dV \tag{7}$$

$${}^{t}_{t}\underline{F} = \int_{{}^{t}V} {}^{t}_{t}\underline{B}_{L}^{T}\,{}^{t}\hat{\underline{\tau}}\,{}^{t}dV \doteq \int_{{}^{t}V} {}^{t}\tau_{ij}\,\delta_{t}e_{ij}\,{}^{t}dV \tag{8}$$

where ${}^{t}_{t}\underline{B}_{L}$ and ${}^{t}_{t}\underline{B}_{NL}$ are the linear and non-linear strain-displacement transformation matrices, ${}^{t}\underline{\tau}$ and ${}^{t}\hat{\underline{\tau}}$ are a matrix and vector of Cauchy stresses and ${}_{t}\underline{C}$ is the incremental stress-strain material property matrix, all referred to the configuration at time t.

2.2 Evaluation of the Constitutive Tensor

Assume that at time t the stresses, strains, and any other important variables are known. In elastic-plastic analysis the stress-strain material

property matrix ${}_t\underline{C}$ uses the elastic stress-strain relations, $\underline{C}^E$, along with a yield condition, a flow rule, and a hardening rule to account for plastic material behavior. The yield condition, ${}^tF$, for the von Mises yield condition and isotropic hardening can be written as

$$ {}^tF\left({}^t\sigma, {}^t\sigma_y\right) = \frac{1}{2}\,{}^tS_{ij}\,{}^tS_{ij} - \frac{{}^t\sigma_y^2}{3} \leq 0 \qquad (9) $$

where ${}^tS_{ij}$ is the deviatoric stress and ${}^t\sigma_y$ is the yield stress at time t. The flow rule expresses the normality condition for plastic strain increments e^P_{ij} as a function of the yield condition ${}^tF$

$$ e^P_{ij} = {}^t\lambda \frac{\partial {}^tF}{\partial {}^t\sigma_{ij}} \qquad (10) $$

or, in matrix form

$$ \underline{e}^P = {}^t\lambda\,{}^t\underline{q} \qquad (11) $$

where ${}^t\lambda$ is a scalar and ${}^t\underline{q}$ for two-dimensional analysis can be obtained from Eq. (9)

$$ {}^t\underline{q}^T = \left[{}^tS_{11} \quad {}^tS_{22} \quad 2\,{}^tS_{12} \quad {}^tS_{33}\right] \qquad (12) $$

During plastic deformation, ${}^tF = 0$ requires

$$ d\,{}^tF = \frac{\partial {}^tF}{\partial {}^t\sigma_{ij}}\,\sigma_{ij} + \frac{\partial {}^tF}{\partial {}^te^P_{ij}}\,e^P_{ij} = 0 \qquad (13) $$

where σ_{ij} is the total stress increment, which can be written in matrix form

$$ {}^{t}\underline{q}^{T}\,\underline{\sigma} = {}^{t}\underline{p}^{T}\,\underline{e}^{P} \tag{14} $$

The matrix ${}^{t}\underline{P}$ $\left(= -\dfrac{\partial {}^{t}F_{P}}{\partial {}^{t}e_{ij}}\right)$ can be obtained from the plastic work per unit unit volume ${}^{t}W^{P}$,

$$ {}^{t}W^{P} = \int_{0}^{{}^{t}e_{ij}^{P}} {}^{t}\sigma_{ij}\; e_{ij}^{P} \tag{15} $$

and can be written

$$ {}^{t}\underline{p}^{T} = {}^{t}H\left[{}^{t}\sigma_{11}\;\; {}^{t}\sigma_{22}\;\; {}^{t}\sigma_{12}\;\; {}^{t}\sigma_{33}\right] \tag{16} $$

where

$$ {}^{t}H = \frac{2}{3}\,{}^{t}\sigma_{Y}\,\frac{d\,{}^{t}\sigma_{Y}}{d\,{}^{t}W^{P}} \tag{17} $$

For perfectly plastic material, ${}^{t}P_{ij} = 0$ and ${}^{t}H = 0$, where for linear strain hardening with tangent modulus E_T, ${}^{t}H$ can be calculated from

$$ \left({}^{t}H\right)^{-1} = \frac{3}{2}\left(\frac{1}{E_T} - \frac{1}{E}\right) \tag{18} $$

Returning to Eq. (14), the stress increments $\underline{\sigma}$ can be found from the total strain and plastic strain increments, $\underline{e}$ and $\underline{e}^P$, and the elastic material property matrix $\underline{C}^E$,

$$\underline{\sigma} = \underline{C}^E \left(\underline{e} - \underline{e}^P \right) \tag{19}$$

The scalar factor ${}^t\lambda$ can be found from Eqs. (11), (14), and (19)

$${}^t\lambda = \left({}^t\underline{q}^T \underline{C}^E \underline{e} \right) \Big/ \left[{}^t\underline{p}^T {}^t\underline{q} + {}^t\underline{q}^T \underline{C}^E {}^t\underline{q} \right] \tag{20}$$

Substitution of Eqs. (11) and (20) into Eq. (19) allows the stress-strain relation for elastic-plastic material to be written

$$\underline{\sigma} = {}_t\underline{C}^{EP} \underline{e} \tag{21}$$

where, the elastic-plastic material matrix ${}^tC^{EP}$ is given by

$${}_t\underline{C}^{EP} = \underline{C}^E - \frac{\underline{C}^E {}^t\underline{q} \left(\underline{C}^E {}^t\underline{q} \right)^T}{{}^t\underline{p}^T {}^t\underline{q} + {}^t\underline{q} \underline{C}^E {}^t\underline{q}} \tag{22}$$

2.3 Evaluation of Stress at Time t+Δt

We assume that the Cauchy stress at time t is known and the strain increments have been calculated from Eq. (5). The large strain plasticity formulation accounts for rigid body rotation on the current stresses using

$${}^t\overset{\nabla}{\tau}_{ij} = {}^t\dot{\tau}_{ij} - {}^t\tau_{ip} {}^t\Omega_{pj} - {}^t\tau_{jp} {}^t\Omega_{pi} \tag{23}$$

where ${}^{t}\overset{\nabla}{\tau}_{ij}$ is the Jaumann stress rate tensor at time t and ${}^{t}\dot{\tau}_{ij}$ is the time derivative of the Cauchy stress tensor evaluated at time t. The spin tensor ${}^{t}\Omega_{ij}$ is defined by

$$ {}^{t}\Omega_{ij} = \frac{1}{2}\left({}_{t+\Delta t}u_{i,j} - {}_{t+\Delta t}u_{j,i}\right) \tag{24} $$

where ${}_{t+\Delta t}u_{i,j}$ is the derivative of the displacement increment with respect to the j^{th} coordinate direction at time $t+\Delta t$. The material relationship used to evaluate the Jaumann stress rate tensor is

$$ {}^{t}\overset{\nabla}{\tau}_{ij} = {}_{t}C_{ijrs}\,{}_{t}e_{rs} \tag{25} $$

and, if small time increments are used, the stress increment over Δt can be found from Eqs. (23) and (25)

$$ {}^{t+\Delta t}\tau_{ij} = {}^{t}\tau_{ij} + {}_{t}C_{ijrs}\,{}_{t}e_{rs} + {}^{t}\tau_{ip}\,{}^{t}\Omega_{pj} + {}^{t}\tau_{jp}\,{}^{t}\Omega_{pi} \tag{26} $$

The final two terms in Eq. (26) are the correction terms to be added to Eq. (21) to obtain the stress increments for finite strain plasticity.

The implementation of these plasticity relations in ADINA is illustrated in the following flow chart:

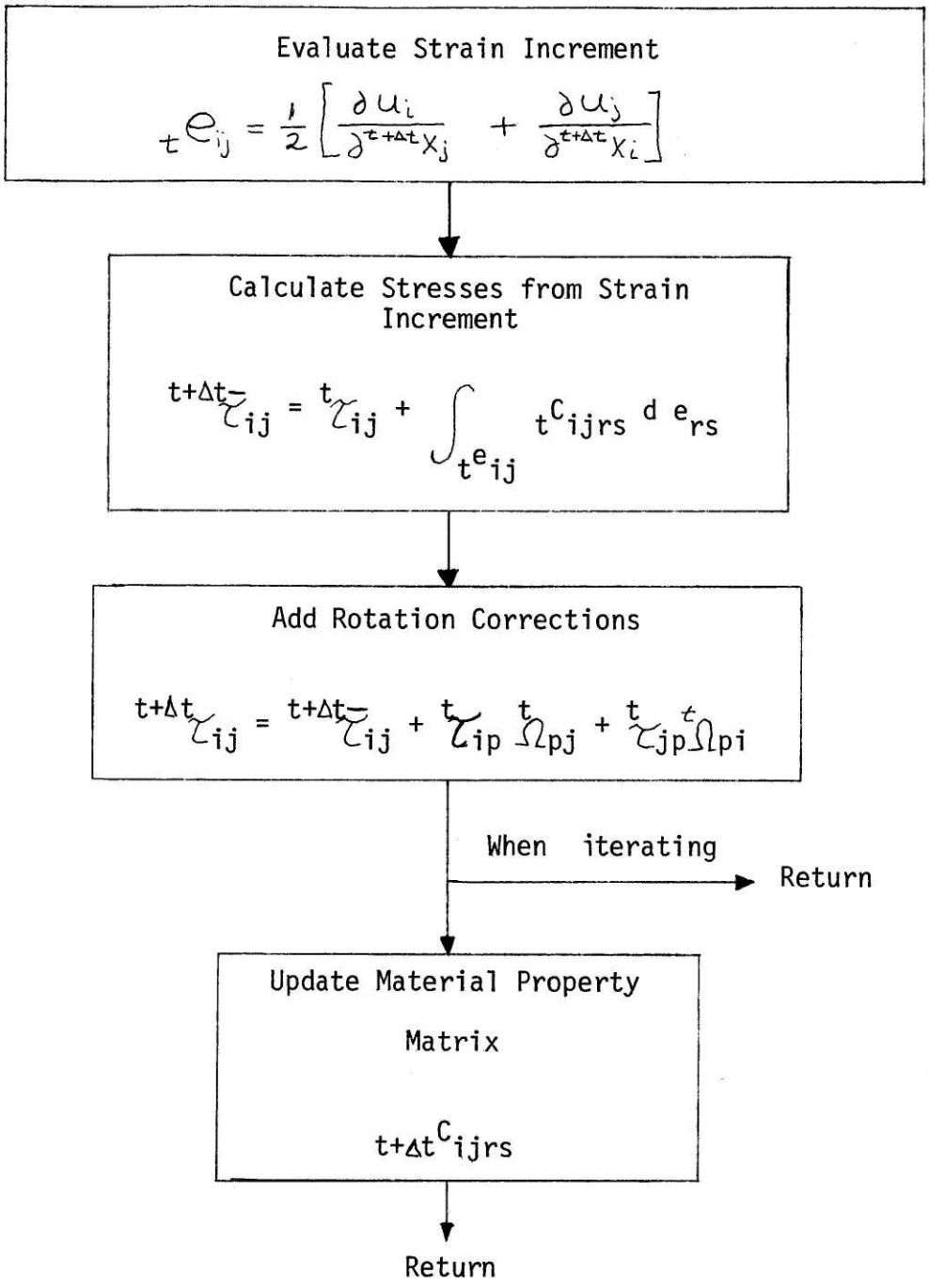
Evaluate Strain Increment
$_{t}e_{ij} = \frac{1}{2}\left[\frac{\partial u_i}{\partial {}^{t+\Delta t}x_j} + \frac{\partial u_j}{\partial {}^{t+\Delta t}x_i}\right]$
Calculate Stresses from Strain Increment
$_{t+\Delta t}\tau_{ij} = {}_{t}\tau_{ij} + \int_{t e_{ij}} {}^{t}C_{ijrs}\, d\, e_{rs}$
Add Rotation Corrections
$_{t+\Delta t}\tau_{ij} = {}_{t+\Delta t}\bar{\tau}_{ij} + {}_{t}\tau_{ip}\,{}_{t}\Omega_{pj} + {}_{t}\tau_{jp}\,{}_{t}\Omega_{pi}$
When iterating
Return
Update Material Property Matrix
$_{t+\Delta t}C_{ijrs}$
Return

2.4 Equilibrium Iteration

The step-by-step solution of the linearized equation of motion, Eq. (4), can be made more effective and efficient through equilibrium iteration during a time step. The equilibrium iteration scheme used in ADINA can be written in matrix form as

$$\left({}^{t}_{t}\underline{K}_{L} + {}^{t}_{t}\underline{K}_{NL}\right)\Delta\underline{u}^{(i)} = {}^{t+\Delta t}\underline{R} - {}^{t+\Delta t}_{t+\Delta t}\underline{F}^{(i-1)} \qquad (27)$$

where $\Delta\underline{u}^{(i)}$ is the displacement increment during the i'th iteration and ${}^{t+\Delta t}_{t+\Delta t}\underline{F}^{(i)}$ can be evaluated from

$${}^{t+\Delta t}_{t+\Delta t}\underline{F}^{(i)} = \int_{{}^{t+\Delta t}V^{(i)}} {}^{t+\Delta t}_{t+\Delta t}\underline{B}_{L}^{(i)^{T}}\ {}^{t+\Delta t}\hat{\underline{\tau}}^{(i)}\ d\,{}^{t+\Delta t}V^{(i)} \qquad (28)$$

similar to Eq. (8). Iteration proceeds until the displacement increments $\Delta\underline{u}$ calculated by Eq. (27) are within a specified tolerance. Solution of the equilibrium equations through iteration over a time step reduces errors caused by the linearization of these equations and prevents the calculated solution from drifting away from the exact solution. In plastic analysis, where the current solution depends on the prior history solution, this is a particularly important consideration. Equilibrium iteration allows larger time steps to be taken without introducing large integration errors and instabilities.

2.5 Sample Solutions

To test the validity of this formulation in predicting large strain behavior, a single, 2-dimensional isoparametric element, with a strain

hardening modulus equal to one-half the elastic modulus, was loaded axially to 30% plastic strain under different boundary conditions. As shown in Figs. 1 and 2, for both one-dimensional and two-dimensional stress situations, the updated Lagrangian formulation follows the path indicated by the material stress-strain law up to large plastic strains. The strain plotted in these figures is the true, logarithmic strain, which is derived from referring displacement increments to the current configuration. The comparison of the updated Lagrangian formulation with analyses accounting for only material non-linearities, as shown in the figures, indicates that a special large strain formulation is needed for plastic strains larger than 5%, as seen in many ultimate load problems. It should be noted that the material non-linear analysis will correctly predict the engineering stress-strain relation (which refers displacement increments to the initial configuration) rather than the logarithmic strain.

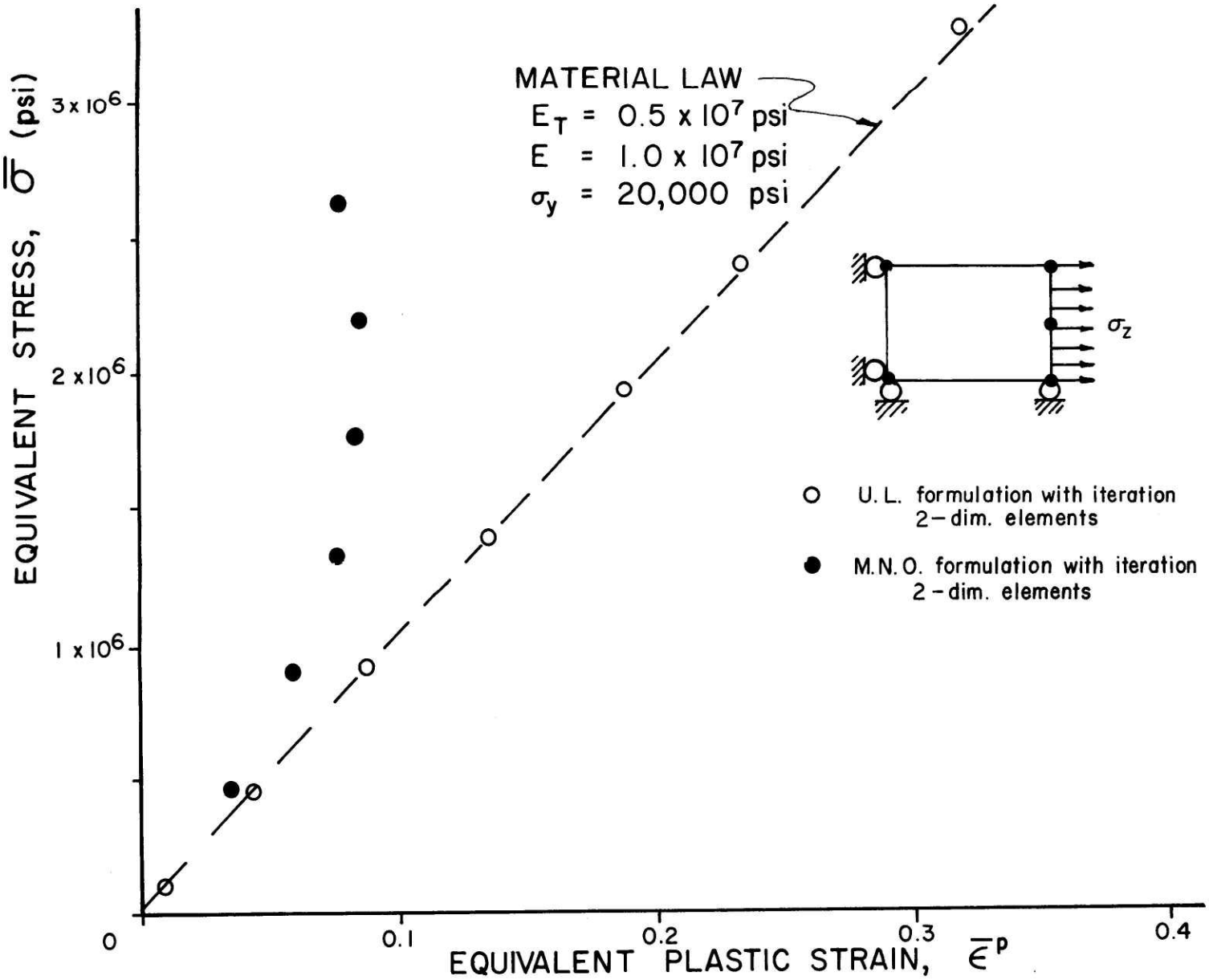

Figure 1. Large Strain Plasticity Solution of One-Dimensional Stress Problem

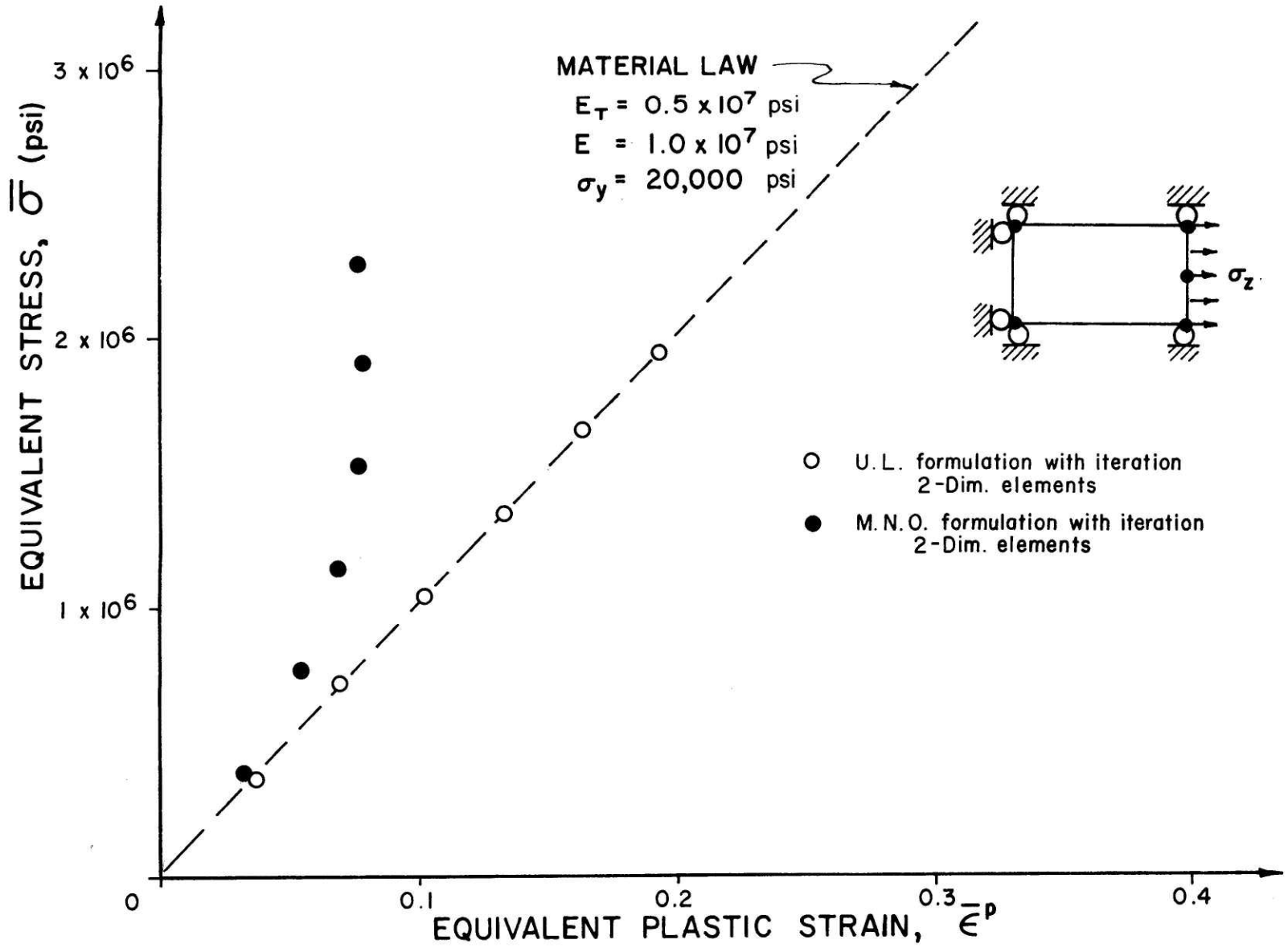

Figure 2. Large Strain Plasticity Solution of Two-Dimensional Stress Problem

3. EFFECT OF INTEGRATION ORDER ON STRESS CALCULATION IN THE FULLY PLASTIC REGION

The inadequacy of some 2-D isoparametric elements in calculating stresses when the element becomes fully plastic has been examined by several investigators. Nagtegaal, Parks and Rice [17] summarized that accurate plasticity solutions depend on the number of kinematic constraints that are present in the deformation modes of an element, and examined the implications of using various 2-D and 3-D isoparametric elements with incompressibility constraints. De Lorenzi and Shih [10] found that the limit load for a beam in bending was correctly predicted using straight-edged, eight-node elements, while the load-deflection curve for the same problem showed no limit load when four node elements were employed. In earlier work, Herrmann [11] observed that the conventional displacement formulation produced poor accuracy in stress calculations for any incompressible or nearly incompressible material (Poisson's ratio close to 0.5) and developed a special constrained displacement formulation for such materials. The incompressibility conditions imposed on an element when plastic strains become large compared with elastic strains necessitates an examination of the appropriateness of the displacement formulation in analyzing large strain plasticity. Naylor [12] investigated the effect of integration order on stress calculations in incompressible, eight-noded isoparametric elements through a number of examples. The study found that the calculated stresses were in close agreement with theoretical values when taken at the 2 x 2 Gauss integration points, but oscillated about the theoretical values when taken at the 3 x 3 integration points. It was also

observed that the average element stresses for 2 x 2 integration were accurate while element averages for 3 x 3 integration showed large errors as Poisson's ratio approached 0.5.

As shown by Nagtegaal et al. [17], the effect of incompressibility constraints on finite element solutions for limit load problems is illustrated by considering the incremental virtual work theorem (Eq. (1a))

$$\dot{\mathcal{R}} = \sum_m \int_{V^{[m]}} \dot{\tau}_{ij} \dot{e}_{ij} \, dV^{[m]} \tag{29}$$

where $\dot{\mathcal{R}}$ is the external virtual work rate (dot indicates time derivative) and $\dot{\tau}_{ij}$ and $\dot{e}_{ij}$ are the stress and strain rates, which are related by the material constitutive relations. The stress rate can be decomposed into a deviatoric rate, $\dot{S}_{ij}$, and a hydrostatic rate, $\frac{1}{3}\dot{\sigma}_{kk}$, using the Kronecker delta δ_{ij}

$$\dot{\tau}_{ij} = \dot{S}_{ij} + \tfrac{1}{3}\delta_{ij}\dot{\sigma}_{kk} \tag{30}$$

The hydrostatic stress rate is tied to the dilatational strain rate by the elastic bulk modulus, κ

$$\tfrac{1}{3}\dot{\sigma}_{kk} = \kappa \dot{e}_{kk} \tag{31}$$

Substitution of Eqs. (30) and (31) into Eq. (29), and introducing the deviatoric strain rate $\dot{e}^D_{ij}$, gives

$$\dot{\mathcal{R}} = \sum_m \int_{V^{[m]}} \left[\dot{S}_{ij} \dot{e}^D_{ij} + \kappa \left(\dot{e}_{kk} \right)^2 \right] dV^{[m]} \tag{32}$$

As the limit load is approached in perfectly plastic conditions, the

deviatoric stress rates will approach zero, but will always be positive (due to the normality conditions for plastic strain increments, see [7]), and Eq. (32) can be written in inequality form when near the ultimate load

$$\dot{\mathcal{R}} \geq \sum_{m} \int_{V^{[m]}} \mathcal{K} \left(\dot{e}_{kk} \right)^2 dV^{[m]} \qquad (33)$$

The limit load is defined as the load at which displacement increments are possible without additional load increment, which is equivalent to saying $\dot{\mathcal{R}}$ goes to zero. By Eq. (33), this is only possible if $\dot{e}_{kk}$ goes to zero throughout the finite element mesh. If this condition is not met, the boundary traction rates will always be positive and no limit load will be reached. For general incompressible materials where the elastic modulus $\mathcal{K}$ goes to infinity, it can be seen immediately from Eq. (32) that $\dot{e}_{kk}$ must vanish everywhere in the mesh or the external work input will be infinite. Therefore, for proper stress calculations (and hence ultimate loads) in incompressible materials (including fully plastic materials as the limit load is approached), the dilatational strain increment $\dot{e}_{kk}$ must be zero everywhere in the finite element mesh.

The Naylor study [12] arrived at a similar observation and noticed that the inaccuracy in stresses is in the mean hydrostatic stress component while the deviatoric components of stress were accurate for all models and integration schemes, a result consistent with the above discussion. The conclusion arrived at by Naylor and later extended by Bercovier [13] to general isoparametric elements ties the accuracy of stress calculations to both the integration order and the total number of degrees of freedom in the model. Specifically, the constraint of zero volumetric strain increment must be satisfied at each integration point. Since the strain increments and nodal displacements are related by the shape functions, Naylor reasoned that the satisfaction of the strain constraints is possible only if the

number of integration points is less than the total number of degrees of freedom (an observation consistent with the results of de Lorenzi and Shih [10]). While this may be a useful rule of thumb for establishing a finite element model, it is not the absolute determinant of whether a model can predict stresses accurately. In plane stress problems, the condition $\dot{e}_{kk} = 0$ can be satisfied regardless of the number of integration points or degrees of freedom. Further, boundary conditions, either applied displacements or tractions, may produce a displacement pattern which satisfies strain constraints. Finally, if a significant portion of the structure remains elastic while large plastic regions develop, as in many limit load problems, incompressibility conditions need to be satisfied in only part of the mesh. Therefore, in plasticity analysis and limit load problems, it is necessary to satisfy the incompressibility condition ($\dot{e}_{kk} = 0$) in the plastic region in order to properly calculate stresses and obtain an accurate load-displacement relationship.

The finite element model and the selection of the optimum integration order for the analysis of ultimate load analyses must account for both the plasticity and elasticity which exist in the structure. The presence of large regions of plastic, incompressible material as the structure approaches the limit load requires satisfaction of volumetric strain constraints. However, the simultaneous presence of a large elastic region makes the use of special incompressibility formulations (e.g. Herrmann [11] and Bercovier [13]) or use of mixed integration schemes (2 x 2 integration on hydrostatic part and 3 x 3 integration on deviatoric part) inefficient. The conventional displacement formulation is sufficiently accurate if certain

kinematic constraints are satisfied, either by reducing the integration order or special arrangement of the finite element model. The effect of reducing integration order on the elastic solution also needs consideration since 2 x 2 Gauss integration introduces a fourth rigid body mode which may be excited during the solution. The determination of the optimum integration order for a particular problem is important in order to obtain accurate limit load results.

4. FINITE ELEMENT ANALYSIS OF PLANE STRAIN PUNCH

4.1 Problem Definition

The example chosen to illustrate the various features of finite element limit load analysis was a rigid, plane strain punch indenting an infinite half space of elastic-perfectly plastic material. The problem is similar to those analyzed in metal working processes and is encountered in foundation analyses [2], [3]. The theoretical solution to the problem is well known and has been determined through different analytical techniques. Hill [14] uses slip-line field theorems to arrive at the limit load. Martin [7] employed upper and lower bound limit theorems and arrived at the same result. Anderheggen [5] used a finite element formulation specially designed for limit analysis and duplicated the results of Hill. The advantages of this example for this analysis include a well documented theoretical result for comparison, the interaction of large plastic and elastic regions, and localized regions of large plastic strains.

The problem geometry is illustrated in Fig. 3. The punch with width 2b is subjected to an applied load P causing it to settle a distance w into the material. The limit load for perfectly plastic material is reached when an increment in settlement can be obtained with no increase in load. The approximate plastic zone shape and slip mechanism as postulated by Hill are also shown in Fig. 3. The theoretical limit load P_{lim} is given by

$$P_{lim} = (2 + \pi)(2b)(k) \tag{34}$$

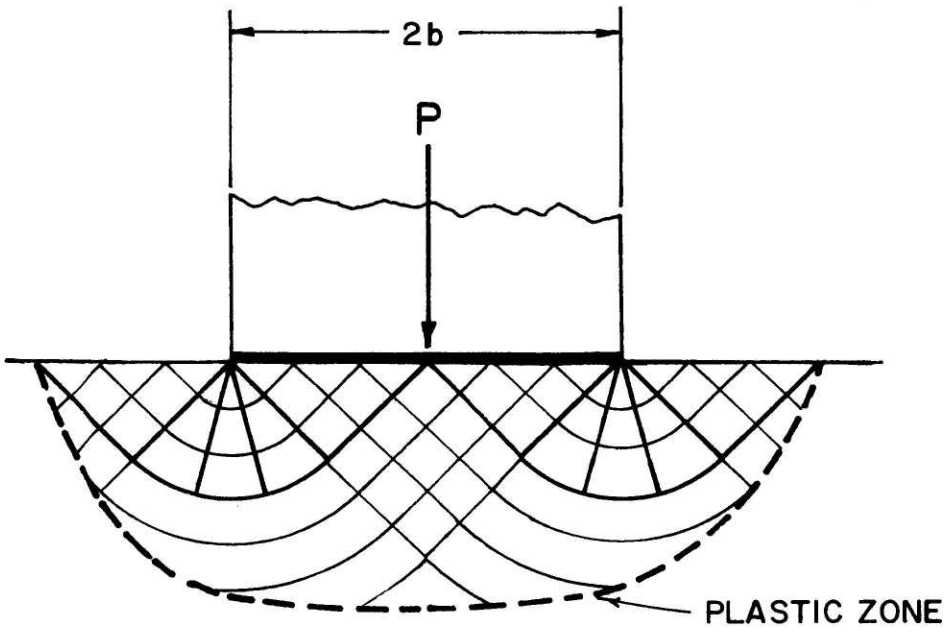

Figure 3. Plane Strain Punch Problem

where k is the critical shear stress for the material and is equal to the uniaxial yield stress divided by $\sqrt{3}$ when the von Mises yield criteria is used.

Two finite element models were used to find the ultimate load: a fine mesh with 160 elements and a coarse mesh with 25 elements. Plane strain conditions were assumed throughout and the symmetry of the problem allowed only half the punch to be modelled. In order to simulate a rigid, flat punch, displacement boundary conditions specifying w were imposed over a distance b from the centerline. The corresponding applied load was found by integrating the stress distribution at a fixed distance below the surface. To account for variations within an element, the average load across an element layer was used rather than the load across an integration point layer. All stresses were determined at the integration points. A small strain analysis (accounting for only material non-linearities) was employed in all cases.

4.2 Fine Mesh

The first finite element model, shown in Fig. 4a, used 160 2-D elements and 366 nodal points for a total of 696 degrees of freedom. The limit load was determined using 2 x 2 and 3 x 3 Gauss integration.

As a test of the element mesh and of the effect of integration order on the elastic solution, the model was used with a point load applied at the centerline. The resulting stress distribution was compared with the Boussinesq solution [18] and the results, taken at a fixed distance below the free surface, are shown in Figs. 5a and 5b. Both integration schemes show good agreement with theory at a distance from the stress singularity, indicating the reliability of elastic solution.

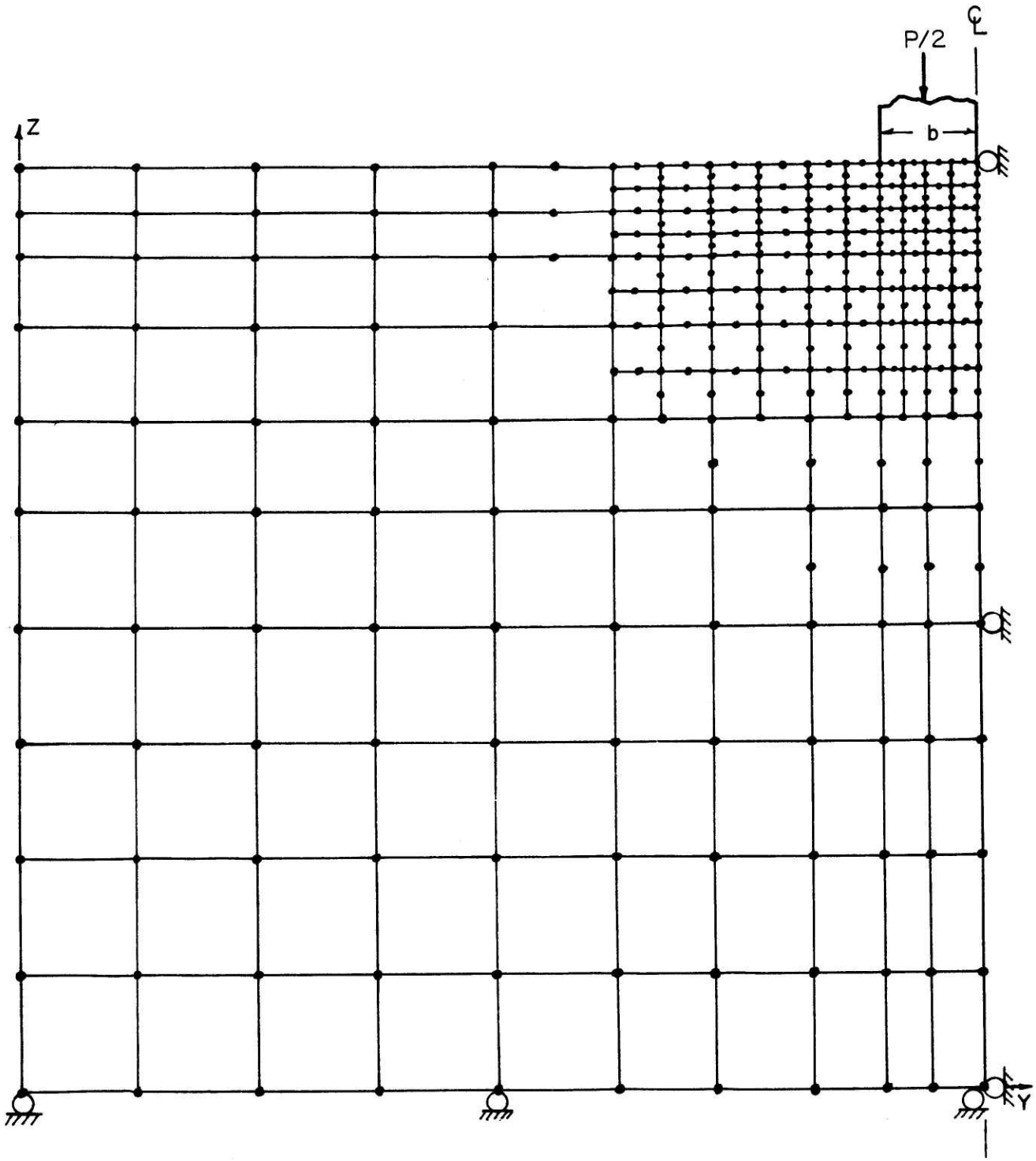

Figure 4a. Fine Mesh Finite Element Model

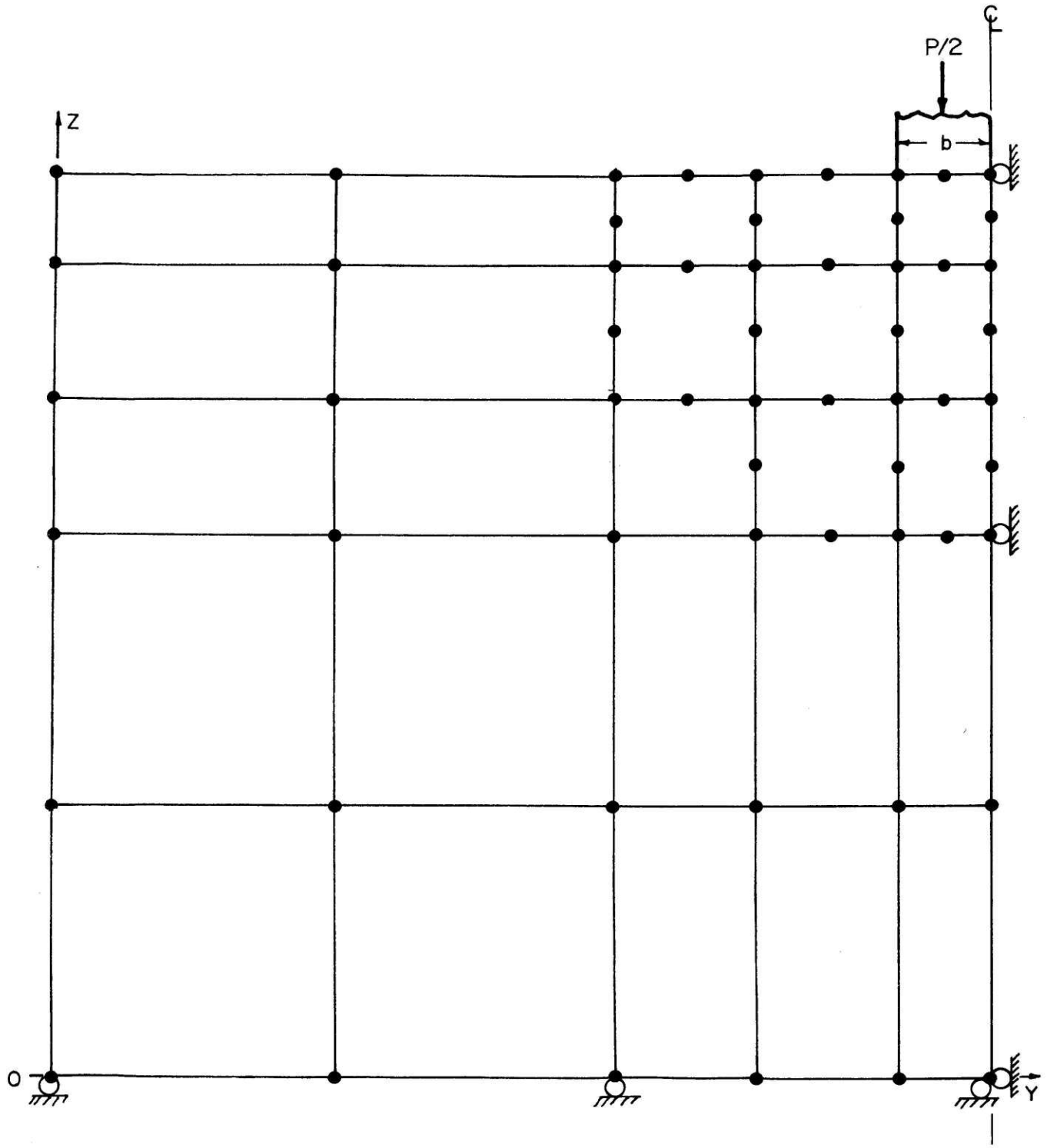

Figure 4b. Coarse Mesh Finite Element Model

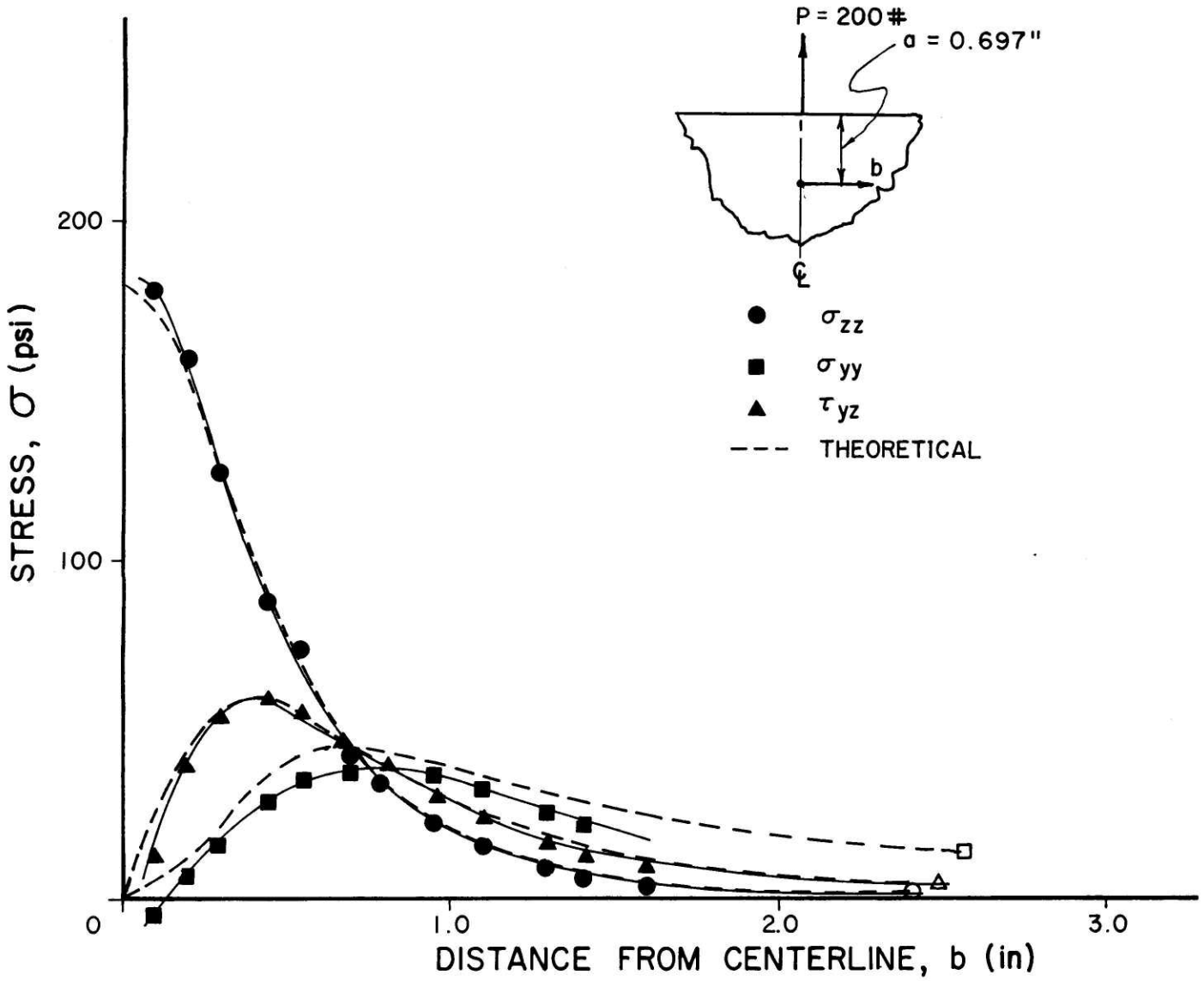

Figure 5a. Finite Element Solution of Boussinesq Problem - 2 pt. integration, fine mesh

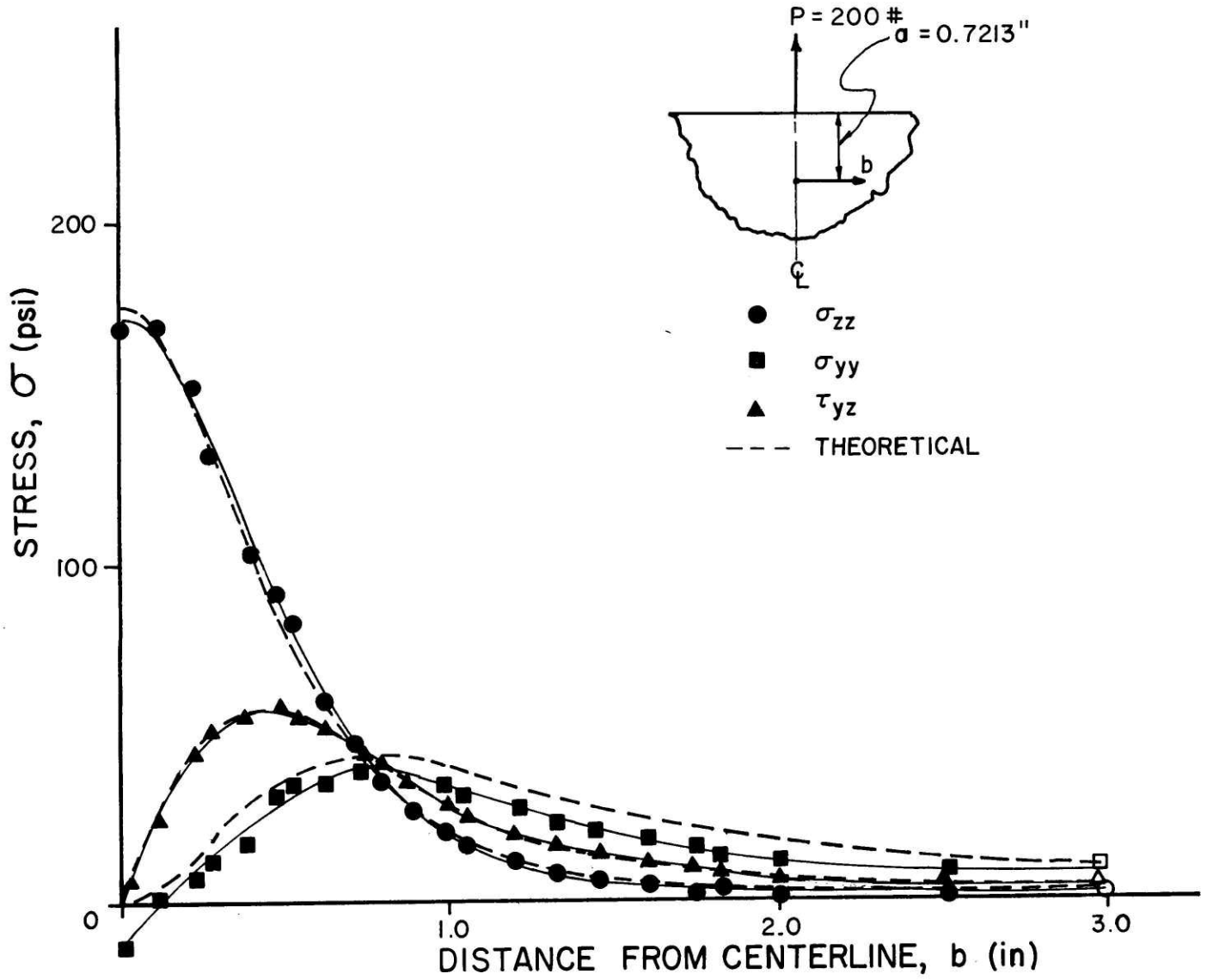

Figure 5b. Finite Element Solution of Boussinesq Problem - 3 pt. integration, fine mesh

The load-displacement curve obtained for the punch problem is shown in Fig. 6. The 2 x 2 integration scheme obtained a normalized limit load $P_{lim}/(2kb)$ of 5.28, only 2.7 percent higher than the theoretical value of 5.14. For 3 x 3 integration, the limit load was higher, $P_{lim}/(2kb)$ reaching 5.62 before leveling off, a value 9.5 percent above the theoretical value. In both analyses, the load-displacement curve did level off and did not exhibit the continuing increase in slope that some investigators noticed in similar problems.

The development of the plastic zone under the punch with increasing settlement is shown in Fig. 7a. The plastic zone growth is very similar in both cases and slightly larger for 3 pt. A zone of plastic material extends a distance of approximately 8b under the punch and extends roughly 3.5 punch widths to either side of the punch. Comparison with the plastic zone size postulated by Hill and shown in Fig. 3 shows that the finite element model predicts a much deeper extent of plasticity under the punch but approximately the same plastic zone width at the surface. The theoretical analysis assumes a slip mechanism extending one to two punch widths below the surface, the finite element analysis agrees with this postulate. The plastic strains calculated by the model were of the order of 10% one punch width deep and dropped to the order of 1% three punch widths down. The plastic strain distribution for 2 x 2 integration at a settlement of (w/b) = 0.2 (when the limit load mechanism is fully established) is shown in Fig. 8a. The magnitude and direction of the strains correspond to the assumed slip mechanism (shown in Fig. 3) used to calculate the theoretical limit load. The three point integration results are similar. Therefore,

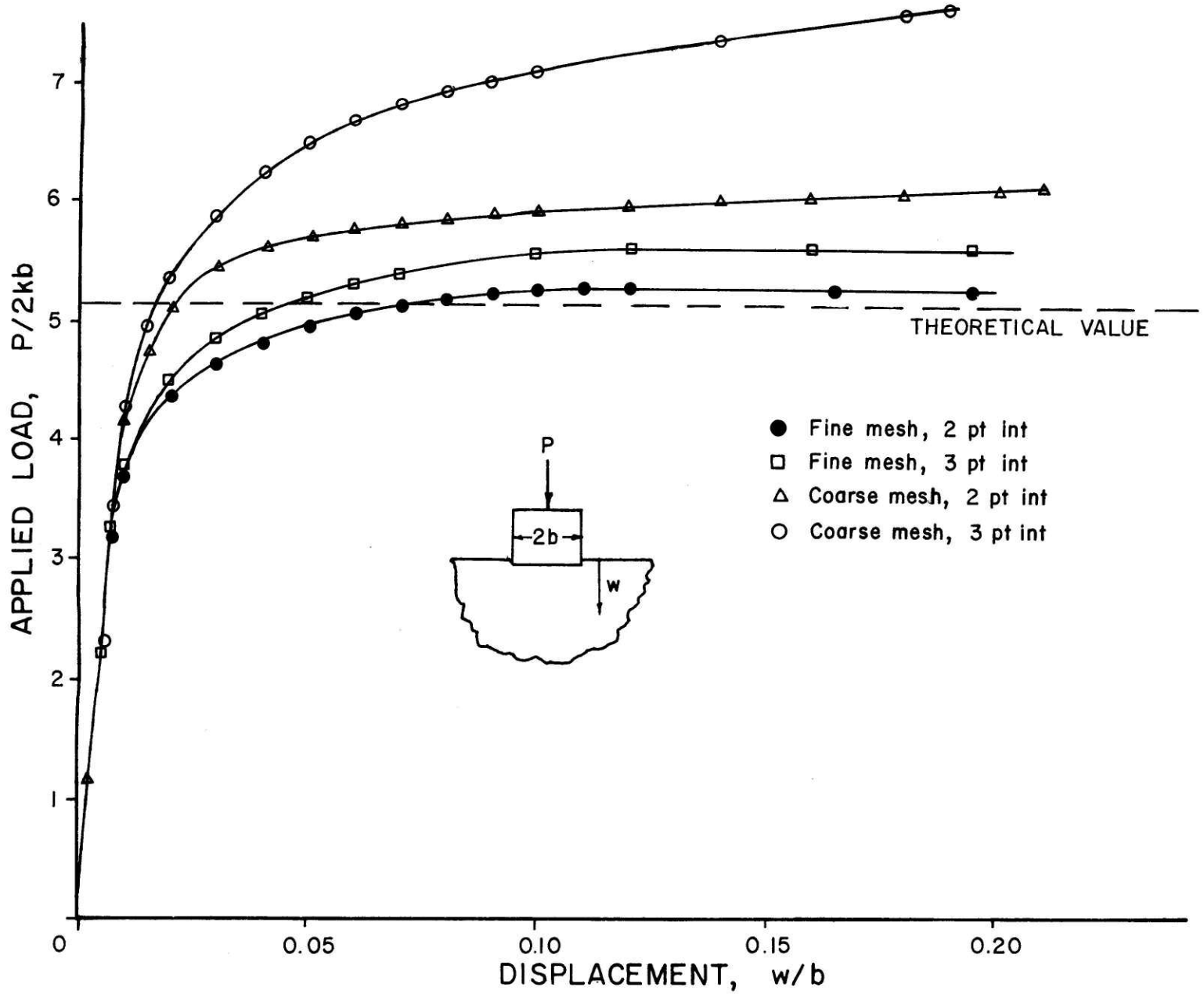

Figure 6. Load-Displacement Curves for Finite Element Model of Punch Problem

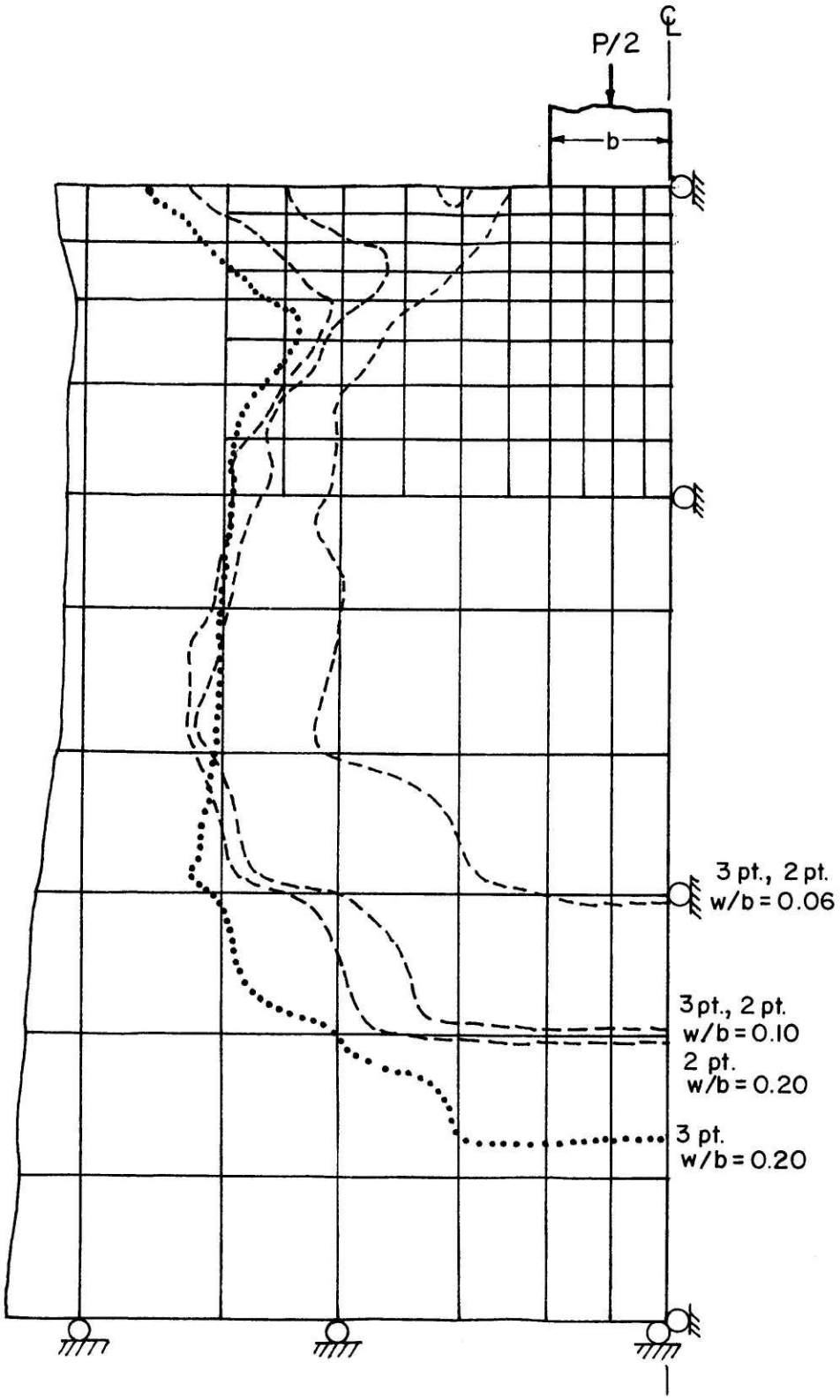

Figure 7a. Growth of Plastic Zone - Fine Mesh

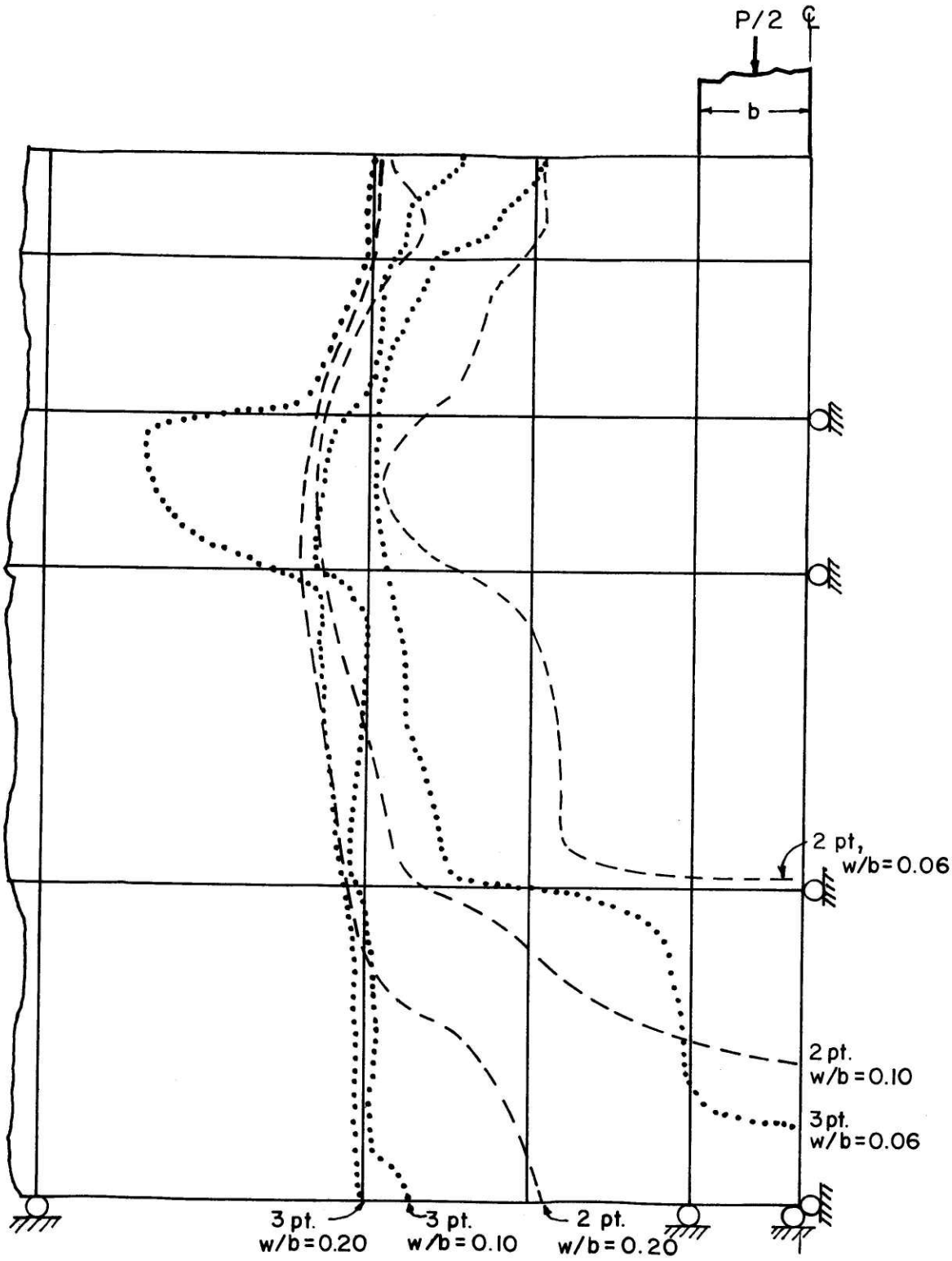

Figure 7b. Growth of Plastic Zone - Coarse Mesh

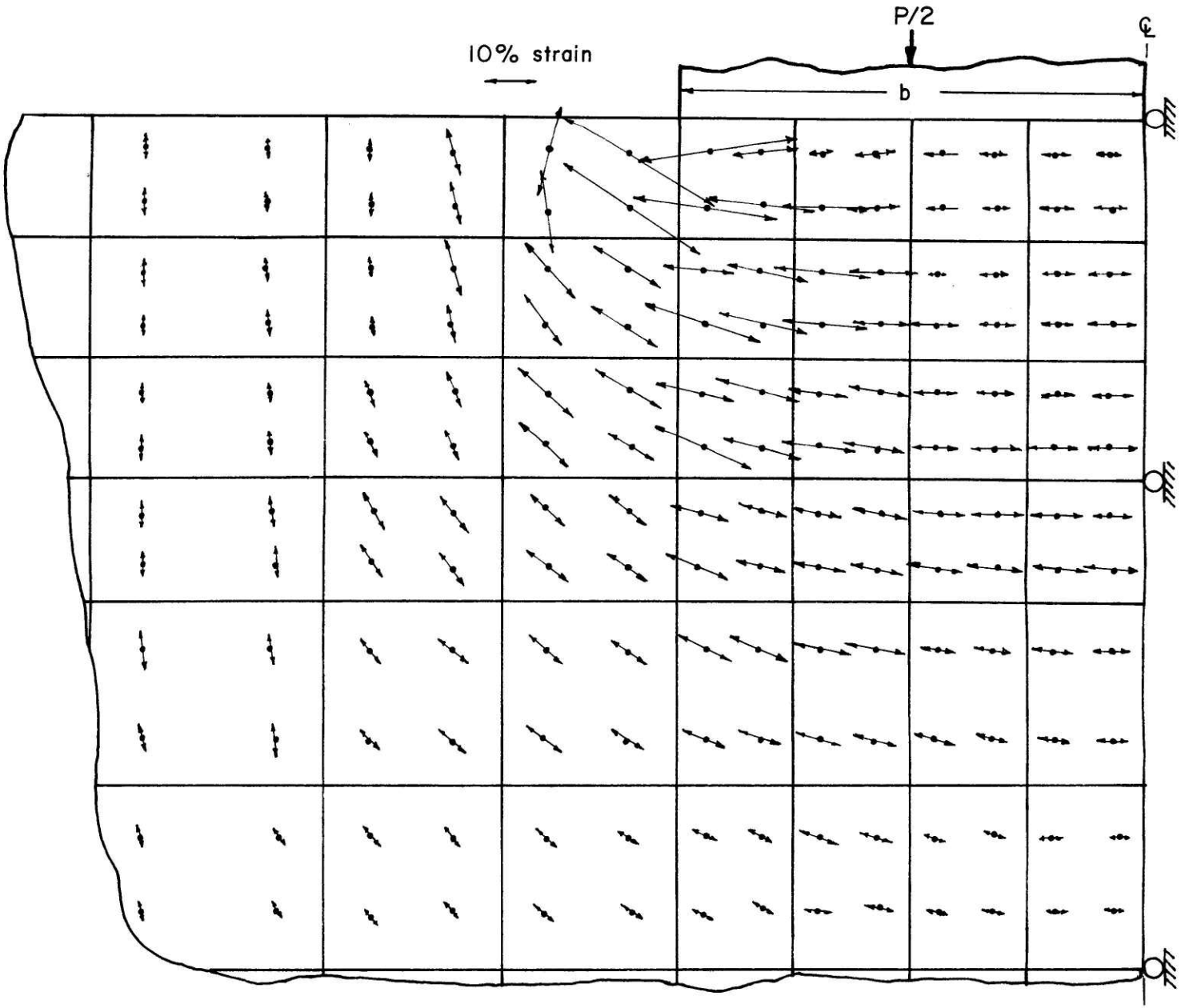

Figure 8a. Plastic Strain Distribution under Punch - Fine Mesh, 2 x 2 Integration

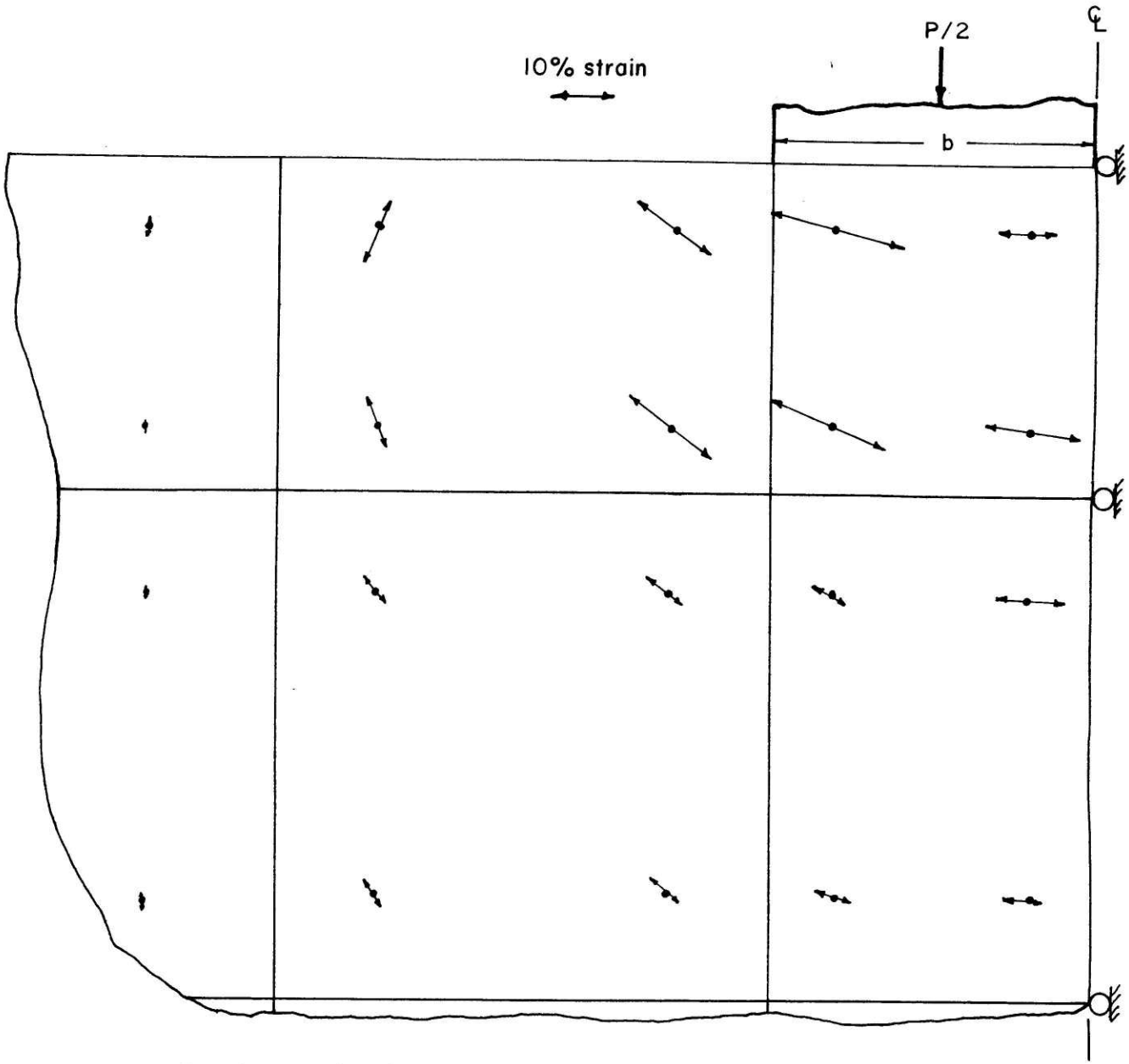

Figure 8b. Plastic Strain Distribution under Punch - Coarse Mesh, 2 x 2 Integration

although the plastic zone size is larger than that assumed by Hill, the slip mechanism and the limit load for the punch problem are adequately modelled using the fine mesh.

4.3 Coarse Mesh

The coarse finite element mesh, Fig. 4b, used 25 2-D elements and 58 nodal points (101 degrees of freedom). It should be noted that this mesh is similar to that used by Yamada and Wifi [2] to analyze footing problems. The load-settlement curves for 2 point and 3 point integration are shown in Fig. 6. Unlike the fine mesh results, the coarse mesh exhibits no limit load, but reaches a terminal slope at large settlements at values much larger than what theory predicts. Again, results for 3 x 3 integration are consistently higher than those for 2 x 2 integration.

Examination of the plastic zone growth, illustrated in Fig. 7b, shows the extent of plasticity all the way through the mesh underneath the punch and extending roughly four punch widths from the centerline. Again 3 x 3 integration predicts a larger plastic region than predicted by 2 x 2 integration. The plastic strain distribution (Fig. 8b) is similar to the pattern found in the fine mesh, but much coarser, particularly near the edge of the punch.

4.4 Analysis

The two questions about this analysis which need to be considered are: (1) Why did the analysis not predict a limit load using the coarse mesh (2 and 3 point integration)? (2) Why did the analysis predict larger limit loads when three point integration was used in the fine mesh than when two point integration was used?

The failure of the coarse mesh to attain a limit load illustrates the inadequacy of the Naylor criteria [12] that accurate stress solutions depend on having fewer integration points than degrees of freedom. As shown in Table 2, three point integration in the fine mesh predicts a limit load

TABLE 2. DEGREES OF FREEDOM AND INTEGRATION POINTS FOR PUNCH MODEL

Finite Element Model	Integration Order	No. of Integration Points	No. of Degrees of Freedom
Fine Mesh	(2 x 2)	640	696
	(3 x 3)	1440	696
Coarse Mesh	(2 x 2)	100	101
	(3 x 3)	225	101

(even though there are twice as many integration points than degrees of freedom) while two point integration in the coarse mesh does not, despite having one more degree of freedom than integration points. From Figs. 7a and 7b it is observed that the plastic region extends entirely through the coarse mesh under the punch, while the plastic region in the fine mesh is entirely surrounded by a compliant, elastic region. In view of the conclusions of Nagtegaal, et al., [17] that accurate plasticity analysis depends on the satisfaction of the kinematic incompressibility constraints, it is possible that the inadequacy of the coarse mesh is due to its inability to satisfy the constraints under the imposed displacement boundary conditions because of the spread of plasticity entirely through the mesh. The

results do demonstrate the inability to quickly determine when a finite element model is appropriate to analyze a limit load problem and points to the need for further investigation.

The loads predicted by three point integration are higher than two point integration loads in both cases due to the displacement constraints present at more points in the mesh. Satisfaction of incompressibility constraints at more points in the mesh constrains the displacement field to a greater extent for three-point integration and tends to drive the loads higher in the plastic solution. From Fig. 6, the load-displacement curves for different integration schemes separate only when plastic regions begin to become large, indicating that the plastic part of the solution is responsible for the larger loads. The similarity of the elastic solution (Boussinesq problem, Fig. 5) for either integration procedure also indicate this point. It should be noted that use of two point integration may not always be the optimum choice, particularly if the fourth rigid body mode (present in only 2-pt. integration) becomes excited in either the elastic or plastic solution. The type of model used and the integration scheme employed will depend heavily on the type of analysis to be performed, universal guidelines for integration order or number of elements are difficult to establish.

Finally some measure of the relative cost of each analysis should be provided. Table 3 indicates the times for different phases of the solution process along with the total solution time on a Control Data Cyber 175, illustrating the trade-off between model refinement and solution cost.

TABLE 3. SOLUTION TIMES FOR PUNCH ANALYSIS

Analysis	Run #	No. of Steps	Updating Load Vector and Stiffness Matrix (sec.)	Solution of Equations (sec.)	Equilibrium Iteration (sec.)	Print Displace-ments (sec.)	Print Stresses (sec.)	Total (sec.)
Fine Mesh (2 x 2)	1	6	9.23	6.42	5.52	1.29	9.10	32.65
	2	12	16.22	12.97	*	2.64	20.06	53.06
	3	12	18.10	13.24	*	2.61	21.01	56.13
	4	16	23.18	17.41	*	1.72	13.89	57.38
	Total	46	66.73	50.04	5.52	8.26	64.06	199.22
			(.335)	(.251)	(.028)	(.041)	(.322)	(1.000)
Fine Mesh (3 x 3)	1	6	11.18	6.30	9.40	1.27	20.36	49.52
	2	9	22.38	9.53	*	1.06	18.90	53.22
	3	28	74.29	29.77	*	2.03	35.38	143.74
	Total	43	107.85	45.60	9.40	4.36	74.64	246.48
			(.438)	(.185)	(.038)	(.018)	(.303)	(1.000)
Coarse Mesh (2 x 2)	1	24	3.28	.70	2.15	.91	6.23	13.53
	2	30	4.11	.88	2.69	1.14	7.79	16.91
	Total	54	7.39	1.58	4.84	2.05	14.02	30.44
			(.243)	(.032)	(.159)	(.067)	(.461)	(1.000)
Coarse Mesh (3 x 3)	1	24	5.38	.71	3.79	.83	12.94	24.33
	2	24	6.70	.70	*	.40	6.49	14.98
	Total	48	12.08	1.41	3.79	1.23	19.43	39.31
			(.307)	(.036)	(.096)	(.031)	(.494)	(1.000)

Figures in parantheses represent fraction of total time.

* indicates that no equilibrium iteration was used due to unloading in some parts of the model.

5. CONCLUSIONS

Accurate finite element analysis of limit load problems may involve consideration of large strains and displacements and satisfaction of incompressibility constraints in plasticity zones. As shown from the example punch problem, careful modelling of a structure is sometimes sufficient to produce accurate results, and proper refinement of the mesh can be more important than the integration scheme used. Thus, ultimate load problems can often be successfully analyzed without going to special incompressibility formulations or linear programming schemes.

The suitability of the displacement formulation (with consideration of large displacements conditions) in solving limit load problems has important implications. The development costs of special purpose programs (e.g. incompressibility formulations) along with their lack of general applicability and relative inefficiency often make such programs undesirable. Special limit load programs, that may be based on linear and non-linear programming schemes, may be more efficient in determining limit loads, but fail to provide information on the failure mechanism, strains, and stresses, including the development of plasticity and slip mechanisms within the structure. While elastic-plastic analysis with the displacement formulation may be costly in the number of steps required to find a solution, the amount of information obtained from such an analysis is much more complete than a linear programming solution provides. When coupled with the generality of the displacement formulation, it appears desirable to use elastic-plastic analysis in limit load problems and invest the effort in the appropriate modelling of the structure.

The development of criteria that assure an "appropriate" model for a limit load analysis requires further attention. With respect to the punch problem, a further investigation of the reasons for the failure of the coarse mesh to predict an ultimate load should be undertaken. The large strain plasticity formulation outlined above should be used to analyze both models and determine the effect of including geometric non-linearities into the modeling of the problem. Finally, the development of some criteria on what integration order, degree of mesh refinement, and finite element formulation (small or large strain) should be used in a particular analysis (without incurring large computational costs or undergoing an expensive trial and error procedure) would be a significant help in ultimate load analysis.

REFERENCES

[1] G.C. Nayak and O.C. Zienkiewicz, 'Elasto-plastic stress analysis. A generalization for various constitutive relations including strain softening', Int. J. num. Meth. Engng., 5, 113-135 (1972).

[2] Y. Yamada and A. Wifi, 'Large strain analysis of some geomechanics problems by the finite element method', Int. J. Numer. Anal. Methods Geomech., 1, No. 3, 299-318(1977).

[3] J. Christian, A. Hagmann, and W. Marr, 'Incremental plasticity analysis of frictional soils', Int. J. Numer. Anal. Methods Geomech., 1, No. 4, 343-375 (1977).

[4] E. Anderheggen, 'Finite element analysis assuming rigid-ideal-plastic material behavior', Limit Analysis Using Finite Elements, ASME, 1-17 (1976).

[5] A. Biron, 'On results and limitations of lower bound limit analysis through nonlinear analysis', ibid., 18-34 (1976).

[6] A. Peano, 'Limit analysis via stress functions', ibid., 67-86 (1976).

[7] J. Martin, Plasticity, MIT Press, Cambridge, Ma., 1975.

[8] D. Hutula, 'Finite element limit analysis of two-dimensional plane structures', Limit Analysis Using Finite Elements, ASME, 35-52 (1976).

[9] K.J. Bathe, 'ADINA: A Finite Element Program for Automatic Dynamic Incremental Nonlinear Analysis', Report 82448-1, Acoustics and Vibration Laboratory, Mechanical Engineering, Dept., MIT, September 1975 (rev. May 1977).

[10] H. deLorenzi and C. Shih, 'On the use of 2D isoparametric elements for calculations in the fully plastic range', Int. J. of Fracture, 13, 507-511 (1977).

[11] L. Herrmann, 'Elasticity equations for incompressible and nearly incompressible materials by a variational theorem', J. Am. Inst. Aeronautics and Astronautics, 3, 1896-1900 (1965).

[12] D. Naylor, 'Stresses in nearly incompressible materials by finite elements with application to the calculation of excess pore pressure', Int. J. num. Meth. Engng., 8, 443-460 (1974).

[13] M. Bercovier, 'Finite elements for incompressible or nearly incompressible materials', Proceedings of ADINA Conferenece, Report 82448-6, Mech. Engng. Dept., MIT, August 1977.

REFERENCES (Cont'd)

[14] R. Hill, The Mathematical Theory of Plasticity, Oxford University Press, London, 1950.

[15] S. Key, J. Biffle, and R. Krieg, 'A study of the computational and theoretical differences of two finite strain elastic-plastic constitutive models', Sandia Laboratories, Albuquerque, 1976.

[16] K.J. Bathe, 'Static and Dynamic Geometric and Material Nonlinear Analysis using ADINA', Report 82448-2, Acoustics and Vibration Laboratory, Mechanical Eng. Dept., MIT, May 1976 (rev. May 1977).

[17] J. Nagtegaal, D. Parks, and J. Rice, 'On numerically accurate finite element solutions in the fully plastic range', Comp. Methods in Applied Mechanics and Eng., 4, 153-177, (1974).

[18] S. Timoshenko and J. Goodier, Theory of Elasticity, McGraw-Hill, New York, 1951.